

Complex Permittivity Measurements with Quasioptical Fabry-Pérot Resonators

B. D. Elwood^{1,2,*}, P. K. Grimes¹, and J. M. Kovac^{1,2}

¹Center for Astrophysics | Harvard & Smithsonian, Cambridge, MA 02138, USA

²Department of Physics, Harvard University, Cambridge, MA 02138, USA

Abstract. As millimeter instrumentalists push the precision and mapping speed of their instruments ever-higher to make ever-deeper measurements, the need for a precise understanding of the complex permittivity of the dielectrics used in these instruments at their operating temperature heightens. To address this need, we have developed high quality factor quasioptical Fabry-Pérot open resonators spanning 75 GHz-330 GHz, optimized for rapid use in a quick-turnaround 4 K cryostat. These hemispherical resonators enable precise metrology of low-loss bulk and thin dielectrics. We present the design and characterization of, and some complex permittivity measurements from, a W-band open resonator.

1 Introduction

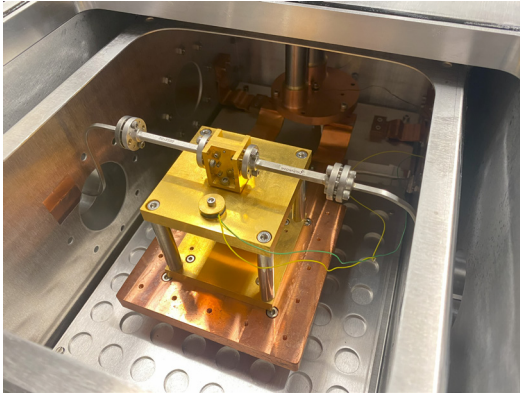
The need for rapid, precise characterization of dielectrics near realistic operating conditions has become apparent in CMB polarimeters that employ cryogenic refractive optics such as the current and upcoming BICEP instruments [1]. Losses in transmissive optics elevate photon noise, degrading mapping speed and overall sensitivity, while scattering from commonly employed foam materials can additionally contribute to undesired environmental coupling. Meeting the stringent demands of these high-contrast, high-throughput imaging systems requires a precise understanding of the complex permittivity of the dielectrics that compose their optics, including laminates and bulk materials. This understanding in turn guides both the selection of materials for optical components and the design of those optical components, including anti-reflection coatings, refractive elements, and radio-transparent multi-layer insulation [2].

Rapid, precise measurements of complex permittivity can accelerate informed material selection in millimeter-wave optics. Beyond CMB instrumentation, this capability is also relevant to a wide range of mm-wave applications, including black-hole imaging experiments, line-intensity mapping, cavity axion searches, and sub-mm surveys [3, 4]. In this work, we introduce and validate an approach based on quasioptical Fabry-Pérot resonators, enabling rapid and precise broadband characterization of low-loss materials.

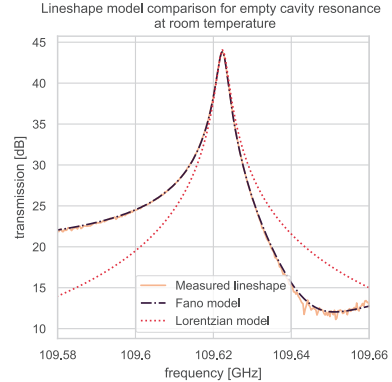
2 Apparatus & Procedure

The mode structure of open resonators contains information about cavity length and loss. Open resonators are inherently broadband. They also exhibit reduced systematic uncertainties associated with sample dielectric dimensions compared to closed waveguide techniques.

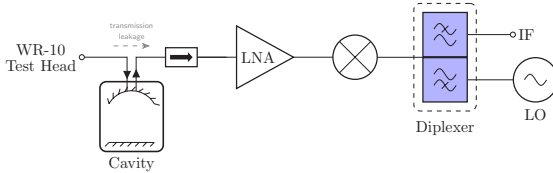
*email: bdelwood@fas.harvard.edu



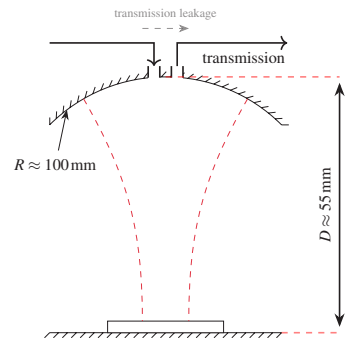
(a) Cavity placed in a quick-turnaround cryostat for cryogenic measurements. We couple in radiation via stainless steel waveguides to decrease thermal conduction from ambient temperature to the cold stages. The cold plate is thermally strapped to the second stage of a PT405 pulse tube cryocooler to cool the cavity down to 4 K. A 50 K radiation shield reduces loading on the second stage.



(b) An example resonance mode measurement (solid peach) overlaid with a best-fit Fano (dash-dot purple) and Lorentzian (dotted red) lineshapes. Note that the asymmetry in the mode due to complex coupling is captured well by the Fano model.



(c) Schematic diagram of the signal chain for W-band measurements [5].



(d) A pictorial diagram of the FP resonator [5].

Figure 1. The Fabry-Pérot resonator employed for this work (a), an example empty cavity measurement (b), the W-band signal chain (c), and a schematic of the FP resonator (d).

Whereas closed waveguide techniques require fabricating multiple samples to span different waveguide dimensions, open-resonator methods allow the same dielectric samples to be used across all bands. Open resonators also permit direct measurement of birefringence via mode splitting, which results from breaking the degeneracy between the polarization eigenstates of the fundamental modes when the cavity is loaded with a birefringent material [6].

The resonator used for this work is constructed from gold-plated, high-purity planar and spherical copper mirrors. These mirrors are separated by Invar struts, forming a hemispherical near-confocal resonator. A VNA extension head couples radiation into the cavity via a split-block waveguide butted into a recess in the top (spherical) mirror. The coupling apertures are sized such that the intrinsic cavity quality factor is $\mathcal{O}(1 \times 10^5)$. A custom receiver composed of an isolator, LNA, and mixer enables S_{21} measurements. The W-band cavity used for the measurements reported in this work has a length of 55 mm and a mirror radius of curvature of 100 mm, giving a free spectral range of approximately 2.7 GHz. A modular design allows

wideband operation by requiring only the replacement of the VNA extension head, spherical mirror, coupling block, and receiver between bands. We have a range of VNA extension heads, coupling blocks, spherical mirrors, and custom receivers for operating cavities from 75 GHz-330 GHz. For loaded cavity measurements, a dielectric sample is pressed against the flat mirror. See Fig. 1 for details on the apparatus.

Inferring loss tangent from a loaded open resonator requires carefully measuring resonance mode frequencies (a measure of cavity length, including sample electrical length) and quality factors (a measure of the energy stored in a given mode). There are two measurement techniques for measuring index and loss tangent: frequency-variation and length-variation [7]. In both methods, we sweep in frequency across the band and record the cavity response. In the frequency-variation method, we fix the cavity length. The modes shift in frequency when the cavity is loaded. With length-variation, we tune the loaded cavity by adjusting cavity length until each loaded resonance returns to its corresponding unloaded frequency. The former approach suffers less from systematic error in measurements of index. The latter is more advantageous for measuring $\tan \delta$, as the frequency-dependent coupling factor $\beta(k)$ – and therefore the intrinsic quality factor $Q_0(k)$ – remains identical in the loaded and unloaded cavities. For both methods:

1. Measure the fundamental mode frequencies and quality factors. Determine the cavity length and mirror radius of curvature from the mode frequencies.
2. Load the cavity with a sample and measure the fundamental modes.
3. In the frequency-variation method, infer the sample electrical length from the shift in mode frequencies. With length modulation, the length change required to retune the cavity gives the sample electrical length.
4. From the empty cavity quality factors, loaded quality factors, and sample electrical length, compute material loss with Eqn. (2).

In the loaded cavity, the wavefront curvature at the mirror and sample interfaces does not match, which shifts the loaded cavity modes relative to a cavity filled with an idealized uniform dielectric slab of the same effective index and loss. The measured loaded mode frequencies, $f_{L,i}$, must therefore be corrected before computing $\tan \delta$:

$$f_L = f_{L,i} \left(1 + \frac{t(n - \Delta)}{n^2 k^2 \omega_t^2 (t\Delta + d)} + \frac{3}{4k^2(t\Delta + d)R} \right) = f_{L,i} (1 + f_{\text{interface}} + f_{\text{mirror}}) \quad (1)$$

where d is the free-space cavity length, R the mirror radius of curvature, ω_t the beam waist at the dielectric interface, n the index of refraction, t the sample thickness, and k the wavenumber in the material. Using the corrected frequencies f_L , we compute the loss tangent as [8]

$$\tan \delta = \frac{1}{Q_s} \frac{2nk(t\Delta + d)}{2nkt\Delta - \Delta [\sin(2(nkt - \Phi_D))]}, \quad (2)$$

where $\frac{1}{Q_s} = \frac{1}{Q_L} - \frac{1}{Q_0(k)}$, with Q_L the loaded quality factor, $Q_0(k)$ the intrinsic quality factor at wavenumber k , and $\Delta \equiv \frac{n^2}{n^2 \cos^2(nkt - \Phi_T) + \sin^2(nkt - \Phi_T)}$. Further,

$$\Phi_T = \arctan\left(\frac{t}{nz_0}\right) - \arctan\left(\frac{1}{nkR_1}\right), \quad (3)$$

$$\Phi_D = \arctan\left(\frac{d'}{z_0}\right) - \arctan\left(\frac{t}{nz_0}\right) - \arctan\left(\frac{1}{kR}\right) + \arctan\left(\frac{1}{kR_2}\right), \quad (4)$$

with $R_1 = t + n^2 z_0^2 / t$, $R_2 = R_1 / n$, $z_0 = \sqrt{d'(R - d')}$, and $d' = d + t/n$. Φ_T and Φ_D essentially capture the Gaussian beam phase shift accumulated in the dielectric-filled region and free-space region of the cavity, respectively [7].

In general, we utilize the frequency-variation method, as it does not require precise control of the cavity length. We characterize the intrinsic quality factor of the empty cavity by fitting a four-parameter Fano lineshape to the fundamental modes observed in the unloaded cavity within the measurement band. We use a Fano lineshape rather than a Lorentzian as interference between the cavity resonance and transmission leakage produces an asymmetric lineshape that is captured by the complex coupling coefficient in the Fano model.

From these fits, we construct the intrinsic quality factor of the empty cavity as a function of frequency, $Q_0(f)$, by interpolation. We then evaluate this function at the loaded-mode frequencies to obtain the corresponding intrinsic empty-cavity quality factor, Q_0 , in the loss tangent calculation. Fig. 2a shows the measured intrinsic Q_0 values and the interpolated $Q_0(f)$ used for the HDPE measurements, while Fig. 1b shows an example resonance mode with Lorentzian and Fano best-fit models.

Since this apparatus is designed for cryogenic index and loss measurements, we must also characterize the intrinsic quality factor down to 4 K. Cavity loss evolves as a function of temperature for several reasons. As the cavity cools, the dimensions of the coupling block change. These changes alter the coupling aperture size, aperture spacing, and the spacing and pressure at the coupler-mirror interface, thereby perturbing the coupling factor β . Additionally, cavity contraction shifts resonance modes, changing their coupling factor; although this should be a subdominant effect, as the shifts are small and the $Q_0(k)$ curve is slowly-varying. Finally, the surface resistivity of the mirrors generally decreases at colder temperatures, driving up Q .

The background of the resonance mode measurements is dominated by direct transmission from the transmit port to the receive port, depicted in Fig. 1c as "transmission leakage" across the cavity. Fig. 2b demonstrates that this transmission leakage is not a product of direct leakage across the apertures on the face of the spherical mirror; this leakage comes from coupling between the apertures of the waveguide-mirror coupling block. This understanding led us to initially expect that the dominant change in the cavity mode structure during cooldown would be due to variations in the background leakage levels from mechanical changes at the coupling block-mirror interface. Specifically, these variations would arise from changes in pressure and spacing at the coupler-mirror interface, which modify the electromagnetic choke between the split-block waveguide coupler and mirror.

However, we observed that the transmission background did not change significantly after the cooldown. In fact, tracking a single mode during unloaded cavity cooldown, the Q rises by 30.4% (Fig. 2c). This effect appears consistent with reduced mirror surface resistivity. Additionally, given the construction of the coupling block-mirror interface, excess pressure on that interface (which may be caused by differential contraction between the mounting hardware and the coupling block material) can distort the mirror. These distortions will couple power out of the fundamental modes into the higher-order modes. Through several cooldown cycles we did not see evidence of mirror-distortion induced higher-order mode structure, nor did we observe additional mirror distortions immediately after thermal cycling.

3 Results

Utilizing the frequency-variation method, we obtain W-band (75 GHz-110 GHz) measurements of the index of refraction and loss of several materials common in mm-wave instrumentation, which are reported in Table 1. The reported uncertainties include variations in the

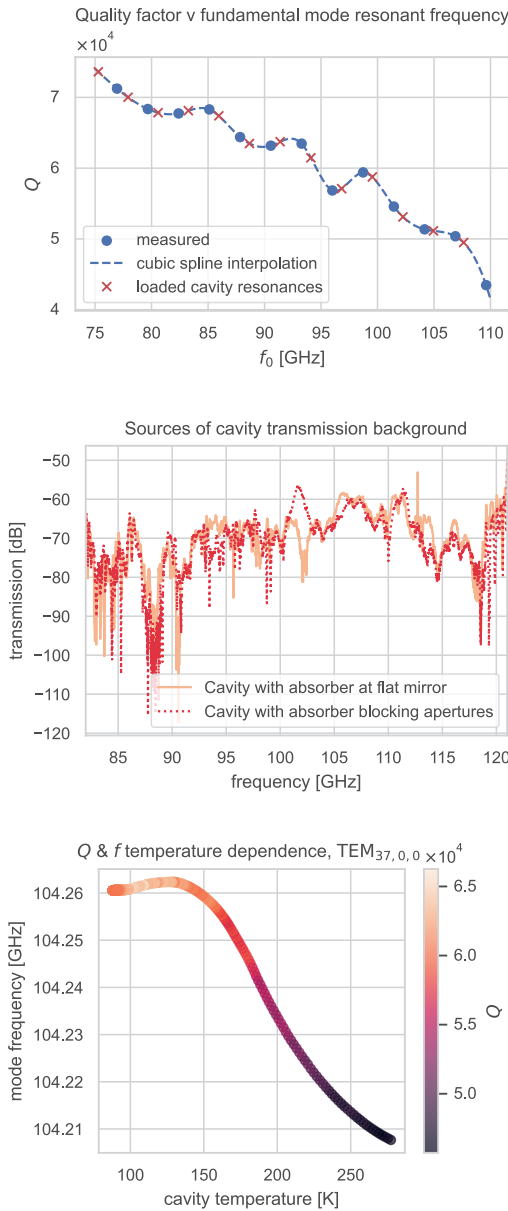


Figure 2. Characterization measurements of the W-band cavity: (a) Intrinsic quality factor as a function of frequency; (b) Broadband transmission with absorbers at different locations; and (c) Mode frequency and Q during cavity cooldown.

mode quality factor and inferred electrical length by measuring the 13 axial modes in the W-band. We also account for systematics due to the measurement procedure by taking multiple measurements of the sample at different orientations and clamping pressures, which helps to control for effects due to sample surface roughness or curvature. As a cross-check for the interface correction (Eqn. (1)), we generally take measurements of several thicknesses of the same material.

(a) The intrinsic cavity quality factor across the WR-10 band at room temperature. The overall downward trend occurs because the near-field attenuation of the evanescent mode coupling of the apertures decreases with frequency, increasing the coupling level. We take the Q_0 in the frequency-variation method from this interpolation.

(b) Broadband scan of the W-band cavity at room temperature. In one scan (peach), the cavity is dampened by an absorber at the flat mirror, while in the other scan (dotted red) an absorber is placed between the coupling apertures on the front side of the spherical mirror. If the background leakage was dominated by coupling between the apertures at the spherical interface, we would expect these two spectra to deviate on the order of 20 dB across the band.

(c) Mode frequency and quality factor for an unloaded cavity during cooldown for a single axial mode. The shift in resonance frequency indicates a length contraction of $15 \mu\text{m}$, consistent with the expected contraction of the Invar struts. The Q of the mode increases $\approx 30\%$, attributed to decreased mirror surface resistance.

Table 1. Indices and losses of several materials at room temperature. The HDPE, annealed HDPE, UHMWPE, and LDPE results were previously reported in [5]. The HDPE, annealed HDPE, and UHMWPE results are reported as the W-band average for 4 sample thicknesses [5]. A measurement of 25 μm thick LDPE is included to illustrate the capability of the cavity to measure thin, low-loss materials. The low-loss silicon results are again reported as the W-band average, but only for a single 3 mm sample. Loss is reported as power lost from the cavity in a single pass through the dielectric (through 2 mm for HDPE, annealed HDPE, and UHMWPE and through 3 mm for Si).

material	n	$\tan \delta (\times 10^{-4})$	loss (dB)
HDPE	1.537 ± 0.003	1.66 ± 0.18	-31
annealed HDPE	1.541 ± 0.004	1.48 ± 0.24	-32
UHMWPE	1.526 ± 0.007	1.43 ± 0.21	-32
LDPE			-52
low-loss Si	3.4230 ± 0.0001	1.47 ± 0.63	-30

4 Conclusions & Future Work

We present a case for the utility of mm-wave open resonators for taking broadband measurements of complex permittivity. We have reported progress on characterizing the unloaded W-band resonator at cryogenic temperatures, and reported index and loss measurements from that cavity at room temperature for samples of HDPE and low-loss silicon.

We are conducting a measurement campaign targeting high-impact candidate materials for optical components in current and future BICEP instruments, with near-term results expected on the room-temperature optical properties of materials for RT-MLI, laminate windows, and AR coatings. In addition to the room-temperature results presented here, future work will focus on extending these measurements to cryogenic temperatures, where dielectric losses and refractive indices are most relevant for CMB instrumentation. Finally, the modular cavity design enables straightforward extension to higher-frequency bands up to 330 GHz, providing a path toward comprehensive permittivity characterization across the mm and sub-mm regimes.

References

- [1] M.A. Petroff *et al.*, in *Millimeter, Submillimeter, and Far-Infrared Detectors and Instrumentation for Astronomy XII* (SPIE, 2024), Vol. 13102, pp. 998–1009
- [2] P.A.R. Ade *et al.*, arXiv:2411.10428 (2024)
- [3] M.D. Johnson *et al.*, *Galaxies* **11**, 61 (2023)
- [4] G. Hoshino *et al.*, *Physical Review Letters* **134**, 171002 (2025)
- [5] B.D. Elwood *et al.*, in *Millimeter, Submillimeter, and Far-Infrared Detectors and Instrumentation for Astronomy XII* (SPIE, 2024), Vol. PC13102, pp. 22–33
- [6] R.G. Jones, *Journal of Physics D: Applied Physics* **9**, 819 (1976)
- [7] P.K. Yu *et al.*, *Proceedings of the Royal Society of London. A. Mathematical and Physical Sciences* **380**, 49 (1982)
- [8] T. Hirvonen *et al.*, *IEEE Transactions on Instrumentation and Measurement* **45**, 780 (1996)